JurnalPolimesin
Department of Mechanical Engineering
State Polytechnic of Lhokseumawe
http://e-jurnal.pnl.ac.id/polimesin
e-ISSN :2549-1999 No. :1 Month :February
p-ISSN :1693-5462 Volume :22 Year : 2024

Article Processing Dates: Received on 2023-07-03, Reviewed on 2023-08-17, Revised on 2023-09-14, Accepted on 2024-01-25and Available online on 2024-02-29

Numerical Study On Characteristics Of the Backward-Facing Step Flow With Variations Of The Slope Angle Of The Step

James Julian*, Rizki Aldi Anggara, Fitri Wahyuni
Program Studi Teknik Mesin, Universitas Pembangunan Veteran Jakarta, Depok, 12450, Indonesia
*Corresponding author: zames@upnvj.ac.id

Abstract
The phenomenon of flow separation plays a vital role in the industrial world. The Backward-Facing Step (BFS) is a general form representing flow separation. This study investigates the influence of the slope angle of the step on BFS flow characteristics at various low Reynolds numbers. According to the CFD results, the flow separation phenomenon forms a circulation zone for each increase in Reynolds numbers. This phenomenon is a result of the sudden expansion of the channel geometry. The BFS with the slope angle of the step demonstrates that the increase in the recirculation zone can be minimized, thus appropriately delaying flow separation. The recirculation zone causes fluid flow to reverse direction, affecting fluid flow efficiency due to resulting pressure differences. Therefore, a BFS with the slope angle of the step exhibits a more efficient flow phenomenon by minimizing the recirculation zone.

Keywords:
BFS, CFD, flow separation, phenomenon, recirculation zone.

1 Introduction

Flow separation has become a topic of discussion because it plays an essential role in various aspects of life. This phenomenon is generally found in various applications, such as airfoils with large angles of attack, spoiler flow, fluid flow through vehicles, and fluid flow through buildings [1]–[6]. The complete application causes flow separation, which has a crucial influence on technological development. A primary geometry that is representative of the flow separation phenomenon is required [7]. In addition, basic geometry can be a theoretical reference for various applications that create complex phenomena. Therefore, the Backward-Facing Step (BFS) is a general representation of the flow separation phenomenon.

Many studies related to the BFS flow have been conducted using experimental and numerical methods with applicable parameters, including separation bubbles, vortex structures, Reynolds stress, pressure coefficients, drag reduction, and geometric design. The BFS is a geometry often used as a test case through internal and external flows. Some studies have investigated incompressible flow through a BFS at high Reynolds numbers [8]. This study used a numerical approach to obtain an efficient solution, which was validated using experimental data. Using the method introduced by Erturk, this study was able to predict the flow separation phenomenon using various parameters with a high degree of accuracy [9]. In addition, other studies have discussed the structure of the mean separation bubbles in a BFS flow [3]. Influence of Reynolds number and expansion ratio on the structure of the mean separation bubble using PIV measurement. This study shows a high-Reynolds-number separation bubble structure that is almost independent of the Reynolds number and expansion ratio. However, the data analysis shows a stream-wise force influence owing to the normal Reynolds stress and significant shear stress. Other studies have focused on channel-flow control behind the BFS using the suction/blowing method [10]. Based on the results of this study, the proposed control method effectively affected the length of the recirculation zone.

The above literature review indicates that the BFS exhibits a complex flow phenomenon. Based on its application, the form of the BFS phenomenon is studied for each role. The stepped geometry is a crucial parameter for studying the resulting flow phenomena. Therefore, this study investigated the influence of the slope angle of the step on the fluid flow characteristics through the BFS. In general, using a BFS with a slope angle plays a significant role in the industrial world. Therefore, the BFS characteristics covered by phenomena in the internal flow or the flow inside the duct are comprehensively explained by applying various applicable parameters. A numerical simulation was chosen as an effective and efficient approach for describing the BFS flow phenomena. Additionally, the influence of the slope angle of the step was tested for each Reynolds number.

2 Research Methods

2.1 Backward-Facing Step (BFS)

The backward-facing step (BFS) is the fundamental geometry that forms the steps because of the sudden expansion of the geometry. BFS flow provides a general feature of the flow separation phenomenon. Flow separation is formed due to the geometry's sudden expansion, making it an essential parameter in various applications [11]. In addition, the BFS can represent essential parameters, including reattachment and multiple recirculating zones. Thus, BFS is a device with a geometry that is of great interest to various researchers.

2.2 Geometries

To illustrate the BFS flow, the change in channel height is defined as the ratio expansion between the upstream channel height (h) and the downstream channel height (H). The expansion ratio used in this study was mathematically regulated by Eq. 1 to form a ladder (S). This study used a different type of step as a comparison model. As shown in Fig. 1, the influence of the variable slope angle of the step is a parameter to be considered when investigating the BFS flow characteristics. The detailed parameters used in this study are listed in Table 1, using the sample expansion ratio from an experimental study by Almary [12].

$$\frac{H}{h} = 1 + \frac{s}{h} \quad (1)$$

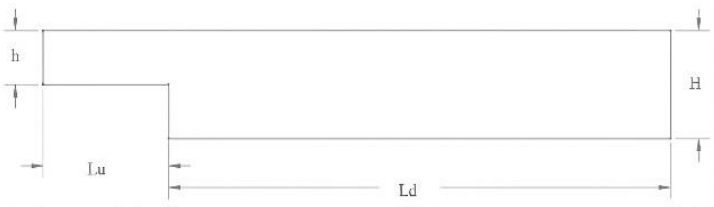

(a) BFS

(b) BFS with the slope angle
Fig. 1. Detail geometries.

Table 1. parameters geometry

Parameter	Value
h/H	1.9423
θ	25°
Lu	2.5 m
Ld	10 m

2.3 Governing Equations

This study chose Computational Fluid Dynamics (CFD) as a numerical approach for solving fluid dynamics cases. The governing equation that plays a role in CFD is the Reynolds Averaged Navier-Stokes (RANS) equation [13]–[27]. To solve the BFS internal flow phenomenon, the RANS equation includes the continuity and momentum equations of the fluid flow. Mathematically, the RANS equation can be expressed as Eq. 2 and Eq. 3.

$$\frac{\partial \rho}{\partial t} + \frac{\partial}{\partial x_i}(\rho u_i) = 0 \tag{2}$$

$$\frac{\partial}{\partial t}(\rho u_i) + \frac{\partial}{\partial x_i}(\rho u_i u_j) = \frac{\partial p}{\partial x_i} + \frac{\partial}{\partial x_j}\left[\mu\left(\frac{\partial u_i}{\partial x_j} + \frac{\partial u_j}{\partial x_i} - \frac{2}{3}\delta_{ij}\frac{\partial u_i}{\partial x_i}\right)\right] + \frac{\partial}{\partial x_i}\left(-\rho\overline{u_i' u_j'}\right) \tag{3}$$

2.4 Mesh and Boundary Conditions

In numerical computation, meshing is an essential part of maximizing the approach used in the research. A quadrilateral mesh was chosen to obtain a structured mesh. As shown in Fig. 2, the boundary conditions indicate the phenomenon of 2D laminar flow through the BFS.

On the upstream fluid domain side, the velocity inlet was defined as the boundary condition with a variation in the Reynolds number, which included Re=50, Re=100, Re=200, Re=300, and Re=400. The selection of the Reynolds number needs to be considered so that there is no influence of the three-dimensional flow that affects the accuracy of numerical computations to produce actual phenomena [28]. Specifically, the inlet velocity is regulated by Eq. 4 – Eq. 6 to fulfil the condition that states a fully developed flow. The outlet was set as a zero-pressure outlet. In addition, the upper and lower walls were set as no-slip walls. In this study, the bottom wall was classified into three areas: upstream, step, and downstream.

$$\mathrm{Re} = \frac{\rho D U_b}{\mu} \tag{4}$$

$$D = 2h \tag{5}$$

$$U_{\max} = \left(\frac{3}{2}\right) U_b \tag{6}$$

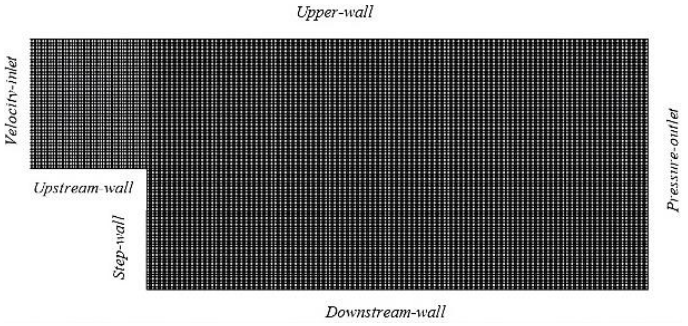

(a) BFS

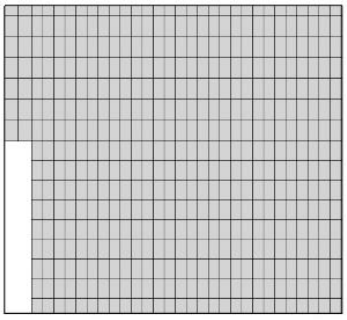

(b) The close-up view of BFS around the step

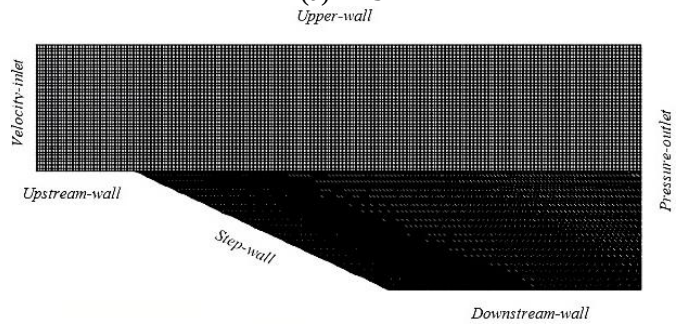

(c) BFS with the slope angle

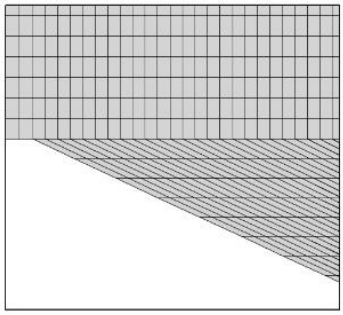

(d) The close-up view of BFS with the slope angle around the step

Fig. 2. Detail mesh and boundary condition.

2.5 Grid Independence Test

A grid-independence test must be performed to ensure the quality of the data generated during the computing process. The grid independence test was performed to determine the mesh with the smallest error value. In this study, the variation in the mesh was determined based on the number of elements, including fine, medium, and coarse meshes. The number of elements for each mesh was 100000, 80000, and 64000, respectively.

The grid independence test process was conducted using the application method in research conducted by Roache [29]. Before the grid independence test, samples with certain variables for each mesh were required. This study determined the velocity of fluid flow at the coordinates x=2.8 and y=0 as comparison data. Furthermore, the first step can be used to determine the ratio at each mesh, regulated by Eq. 7. In the second step, the order value is calculated using Eq. 8. The next step is to determine the error value for the mesh variation using the Grid Convergence Index (GCI) in Eq. 9 and Eq. 10. GCI_{fine} is defined as the error value between the fine and medium meshes. GCI_{coarse} is defined as the error value between the medium and coarse meshes. In addition, GCI calculations must be considered so that the results obtained are in the convergence area. The error value for each mesh variation was determined in the final step. In Table 2, the results of the grid independence test indicate that the fine mesh has a

minor error value. Thus, a fine mesh was selected to continue the computational process.

$$r = \frac{h_2}{h_1} \tag{7}$$

$$\bar{p} = \frac{\ln\left(\frac{f_3 - f_2}{f_2 - f_1}\right)}{\ln(r)} \tag{8}$$

$$GCI_{fine} = \frac{F_s \,|\in|}{\left(r^{\bar{p}} - 1\right)} \tag{9}$$

$$GCI_{coarse} = \frac{F_s \,|\in| \, r^{\bar{p}}}{\left(r^{\bar{p}} - 1\right)} \tag{10}$$

$$\in = \frac{f_{n+1} - f_n}{f_n} \tag{11}$$

$$\frac{GCI_{coarse}}{GCI_{fine} r^{\bar{p}}} \approx 1 \tag{12}$$

$$f\,r_{h=0} = f_1 + \frac{(f_1 - f_2)}{\left(r^{\bar{p}} - 1\right)} \tag{13}$$

Table 2. Grid independence test

Mesh	Fine	Medium	Coarse
Velocity	0.00199549	0.00199600	0.00199779
	5.621803235		
r	1.25		
GCI_{fine}	0.013%		
GCI_{coarse}	0.0447%		
	0.001995286		
	1		
Error	0.01020%	0.03576%	0.12537%

3 Results and Discussion

3.1 Validation

In this study, numerical calculations were used as a more efficient approach than experimental ones. However, the numerical approach has several disadvantages, so the actual quality of the resulting data must be considered. Therefore, a validation process is required to prevent the numerical calculation process from producing actual data. Validation was performed by comparing the samples of the variables produced by the numerical calculation results with the experimental results. For comparison, experimental data were obtained based on the related research by Almary [12]. Changes in the location of the reattachment point for each increase in Reynolds number were selected as samples to compare the numerical results with the experimental results. As shown in Fig. 3, the data generated through the numerical calculations are similar to the experimental data. In addition, the trend shown in the two variables indicates an almost linear increase in the location of the reattachment point with an increase in the Reynolds number. Thus, the data generated through the numerical calculations can be validated to describe the actual phenomenon.

3.2 Analysis

This study investigated the influence of the slope angle of the step on the BFS flow characteristics. In addition, the BFS flow was tested by varying the Reynolds number Re to 50, 100, 200, 300, and 400 to provide a broad understanding of the characteristics of the BFS. Fig. 4 shows the contour velocity magnitude. Fig. 4 shows the flow in the upstream channel; the flow conditions indicate a fully developed flow. It can be observed that there is a significant decrease in velocity when the fluid flow approaches the wall owing to the influence of viscosity. In addition, the fluid flow in the center of the upstream region showed a maximum velocity with a symmetrical profile to the upper and lower walls. This indicates that the two boundary layers developed and merged to satisfy the fully developed flow conditions. Furthermore, the flow through the BFS forms a flow-separation phenomenon. Flow separation occurs because of the sudden expansion of the BFS, which causes the fluid flow to lose momentum to follow the geometry of the channel. In addition, the Reynolds number has a crucial influence on flow separation growth. Therefore, Fig. 4 shows an increase in flow separation with an increase in Reynolds number. However, the BFS geometry with the slope angle of the step exhibits a different behavior. Based on the results of the numerical computation, the zone of flow separation formed can be significantly minimized. This is indicated by the influence of the sudden expansion on the BFS flow, which can be minimized. Therefore, the fluid has sufficient momentum to flow according to the geometry of the channel [30].

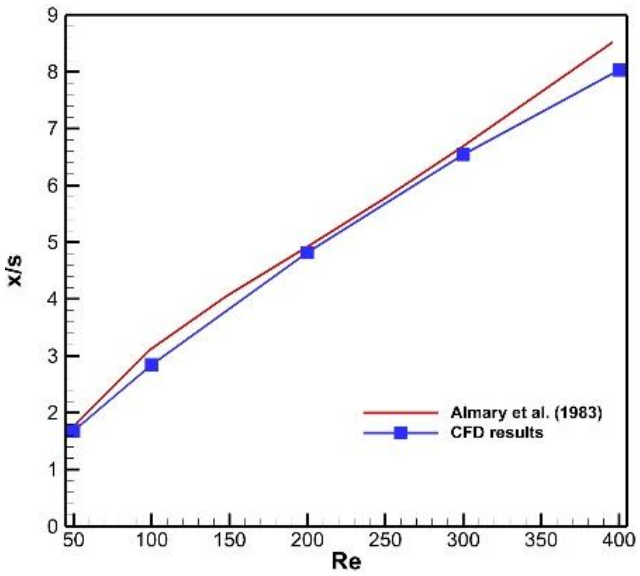

Fig. 3. The location of the reattachment point normalized by the step height S.

In addition, the x-velocity profile is shown at each x-coordinate, as shown in Fig. 5. In the upstream area, both variables show a parabolic curve in the x-velocity profile, indicating that the regulated flow meets the fully developed conditions. Fully developed flow conditions indicate that the two boundary layers formed on the upper and lower walls merge to make the viscosity effect more comprehensive in each zone. When the fluid flow passed through the steps, the x-velocity profile exhibited different characteristics. The x-velocity profile shows an increase in the x-velocity in the opposite vector direction in the flow separation area. This condition triggers a recirculation zone which affects fluid flow in the channel. In the BFS flow with a slope angle of the step, the x-velocity profile, which shows a negative vector, is only visible when Re>100. The fluid flow, which is separated on the downstream side, slowly decays again and forms a boundary layer near the wall such that the fluid outside the boundary layer experiences acceleration. The

interaction of the fluid flow with the wall that forms the boundary layer further expands and recombines. Thus, the x-velocity profile becomes uniform, indicating that the fluid flow is in a fully developed hydrodynamic condition.

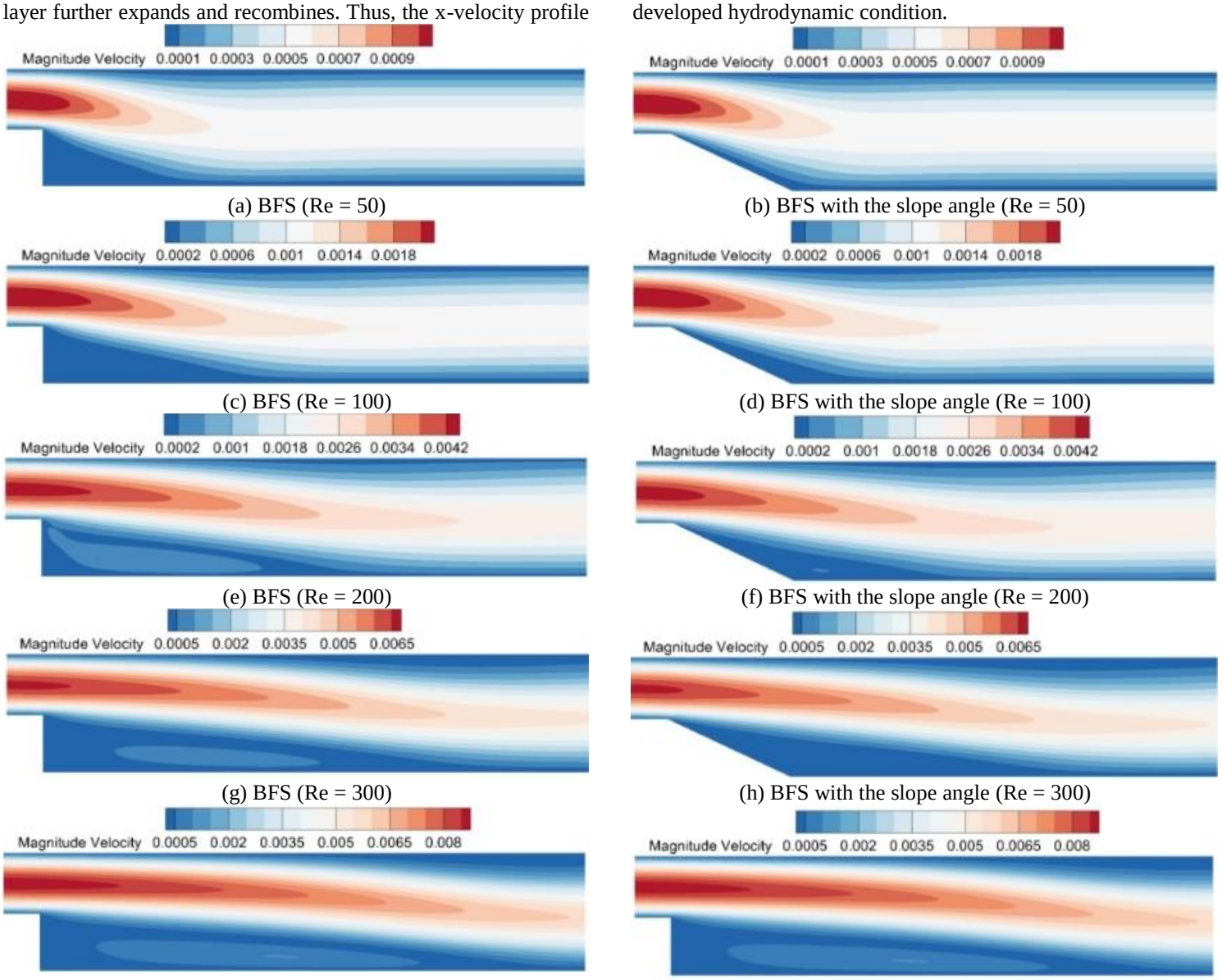

(a) BFS (Re = 50) (b) BFS with the slope angle (Re = 50)

(c) BFS (Re = 100) (d) BFS with the slope angle (Re = 100)

(e) BFS (Re = 200) (f) BFS with the slope angle (Re = 200)

(g) BFS (Re = 300) (h) BFS with the slope angle (Re = 300)

(i) BFS (Re = 400) (j) BFS with the slope angle (Re = 400)

Fig. 4. Magnitude velocity contour of BFS flow.

Furthermore, a streamlined contour investigated the fluid flow pattern through the BFS in more detail. Fig. 6 shows that the flow separation that occurs in the flow through the BFS produces a recirculation zone which forms a negative vector with an x-velocity profile. The growth of the recirculation zone continued to increase with the Reynolds number. Providing a slope angle for the step can significantly affect the flow pattern. At Re=50, the flow pattern on the BFS with slope angle exhibited an ideal fluid flow phenomenon. The flow separation effectively disappears, so that the fluid flow can follow the geometry of the channel. However, this condition could not be maintained as the Reynolds number increased. At Re=100, it can be seen that there is a corner vortex that appears due to vector changes in the fluid flow on the side of the corner step. In addition, a recirculation zone began to appear when Re > 100 and continued to grow as the Reynolds number increased.

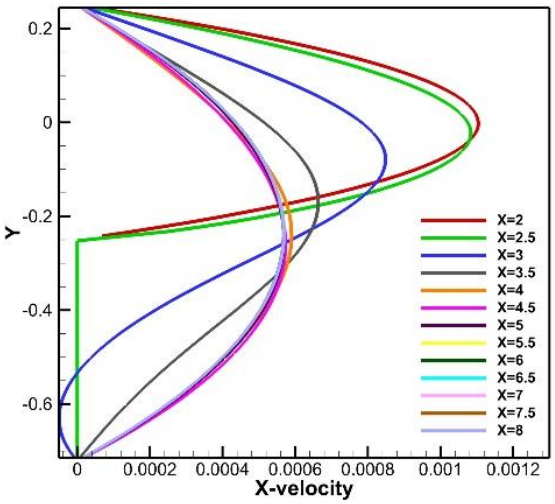

(a) BFS (Re = 50)

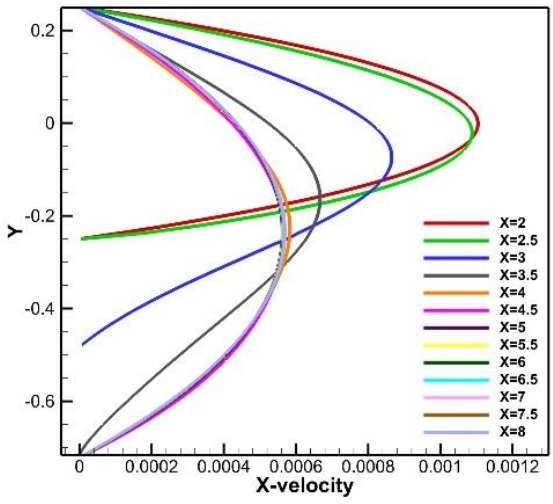

(b) BFS with the slope angle (Re = 50)

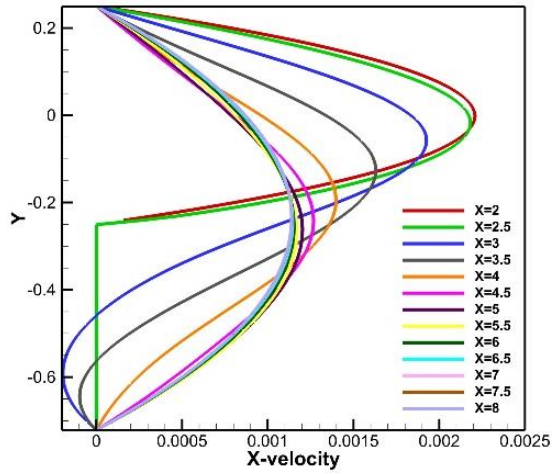

(c) BFS (Re = 100)

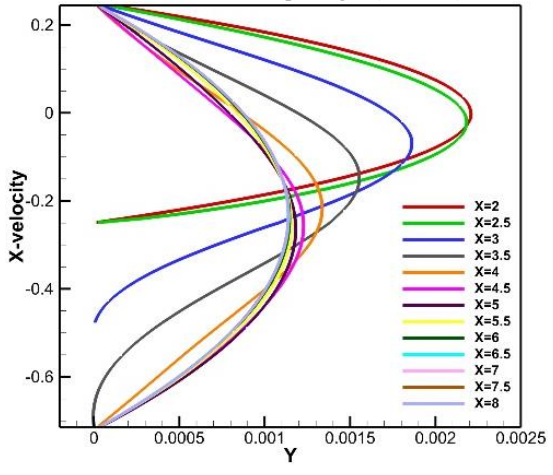

(d) BFS with the slope angle (Re = 100)

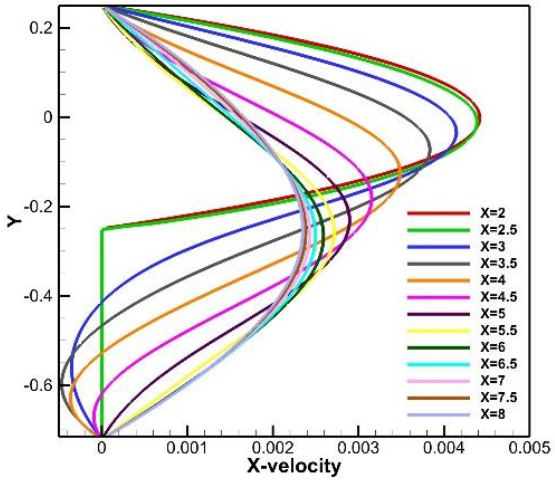

(e) BFS (Re = 200)

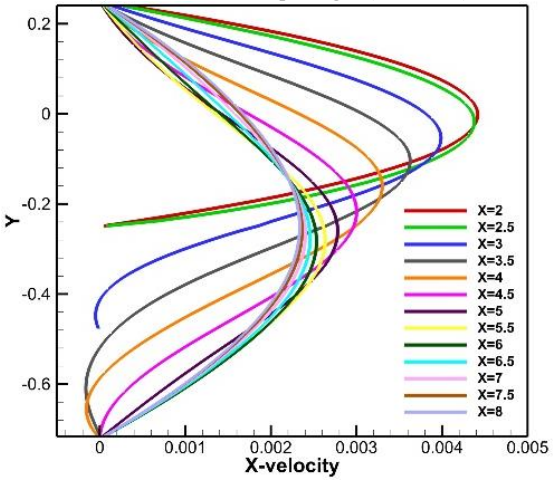

(f) BFS with the slope angle (Re = 200)

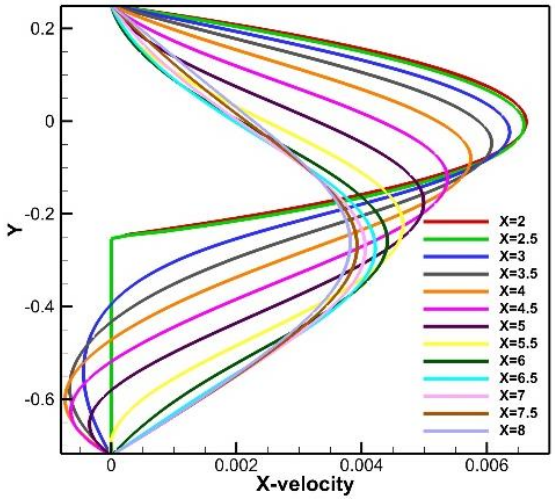

(g) BFS (Re = 300)

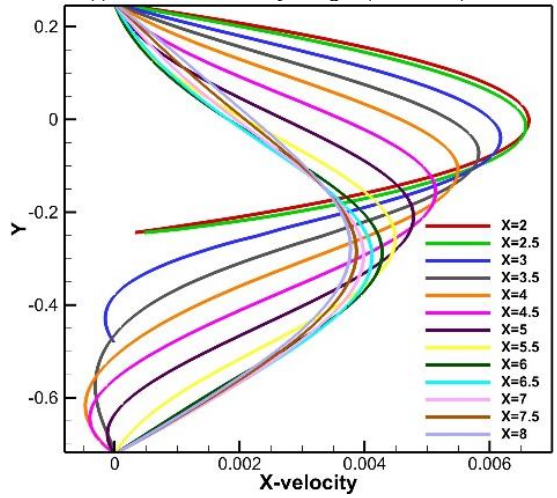

(h) BFS with the slope angle (Re = 300)

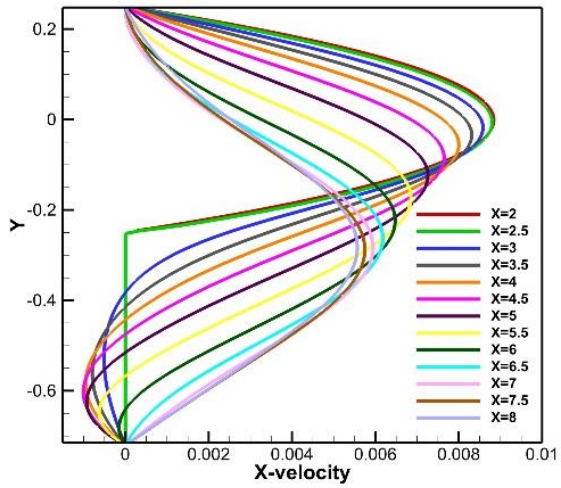

(i) BFS (Re = 400)

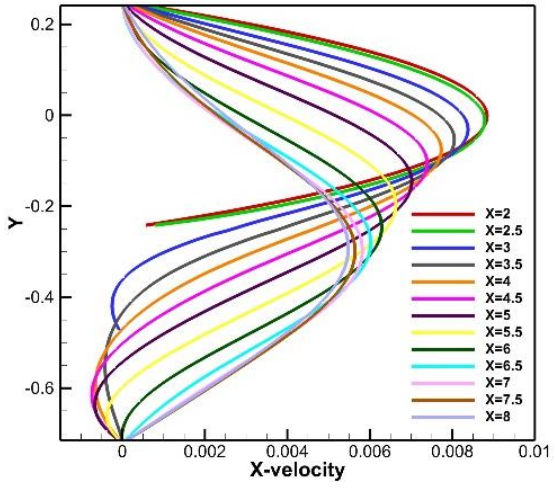

(j) BFS with the slope angle (Re = 400)

Fig. 5. X-velocity profile.

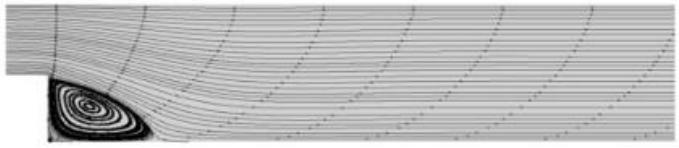

(a) BFS (Re = 50)

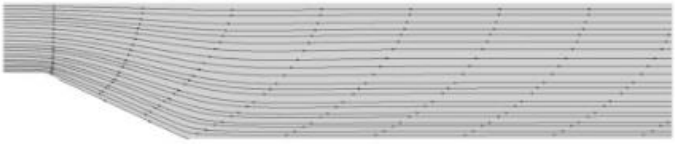

(b) BFS with the slope angle (Re = 50)

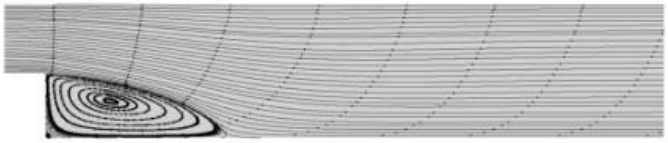

(c) BFS (Re = 100)

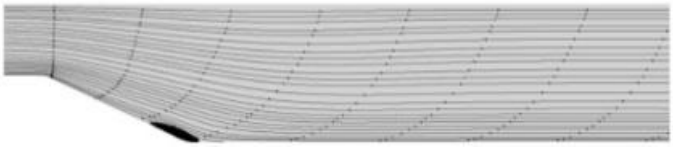

(d) BFS with the slope angle (Re = 100)

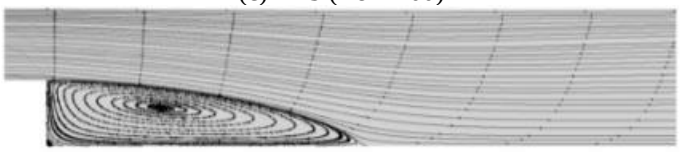

(e) BFS (Re = 200)

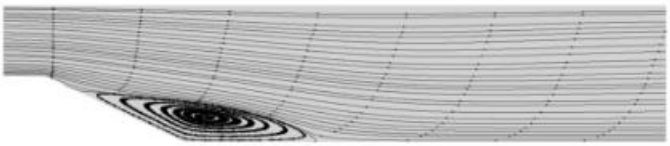

(f) BFS with the slope angle (Re = 200)

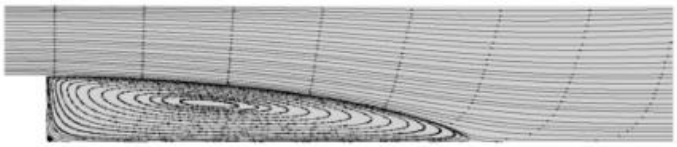

(g) BFS (Re = 300)

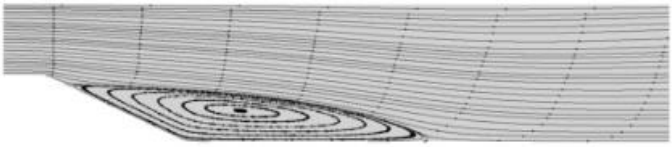

(h) BFS with the slope angle (Re = 300)

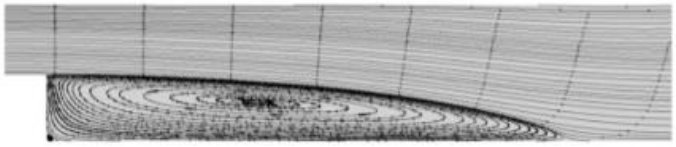

(i) BFS (Re = 400)

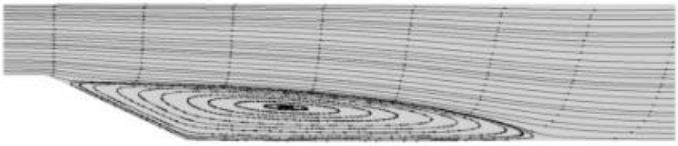

(j) BFS with the slope angle (Re = 400)

Fig. 6. Streamline contour of BFS flow.

BFS with a slope angle effectively minimized the growth of the recirculation zone. This condition can be indicated by two parameters: the flow separation decay and reattachment point. Fig. 7 shows the distribution of the friction coefficient at the normalized step slope for each increase in the Reynolds number with respect to the x-coordinates. The friction coefficient is used as a variable that determines the ability of a BFS with a slope angle to delay the flow separation. Through the friction coefficient, flow separation occurred when it was marked by a decrease in the value of the friction coefficient close to zero. Based on Fig. 7, it is proven that a BFS with a slope angle can delay the flow separation. The flow separation point reached the end of the upstream wall as the Reynolds number increased.

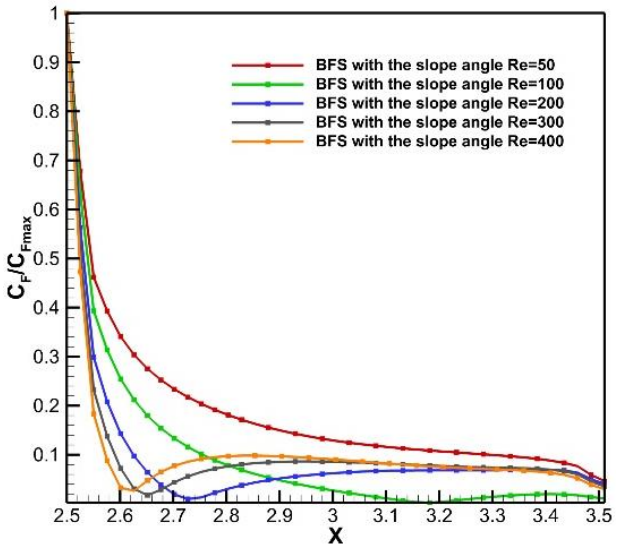

Fig. 7. Graph of C_F normalized by C_{Fmax}.

In addition to delaying flow separation, the size of the recirculation zone can also be minimized. Fig. 8 shows the reattachment point with an increase in the Reynolds number. The point at which fluid flow returns to interact with the wall after flow separation is also known as the reattachment point. In the BFS flow, there was an almost linear increase in the size of the recirculation zone with increasing Reynolds number. In contrast, a BFS with a slope angle showed a shorter reattachment point. Therefore, a BFS with slope angle produces a smaller recirculation zone for each increase in the Reynolds number.

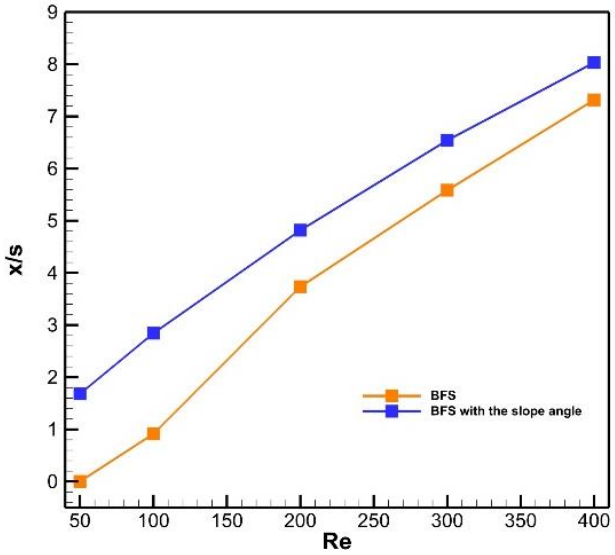

Fig. 8. The location of the reattachment point normalized by the step height S.

In addition, the normalized pressure coefficient distribution along the lower wall, including the upstream and downstream walls, is shown for each increase in Reynolds number in Fig. 9. The resulting recirculation zone has a significant influence on the pressure coefficient distribution. On the upstream wall side, the maximum pressure was reached at the inlet, which caused a linear pressure drop. Each Reynolds number exhibits a different pressure drop gradient. These conditions were identical for both test variables. However, when approaching this step, there was a sharp decrease in the pressure coefficient. At Re= 50 and 100, the lowest pressure coefficient was achieved by BFS without the slope angle. At Re>100, the pressure coefficient was achieved by a BFS with slope angle. Based on Bernoulli's principle, this is triggered by a profile showing high velocity in the BFS with a slope angle towards the step. On the downstream side, the pressure coefficient increased becauseof the resulting recirculation zone. In the recirculation zone, the fluid flow experiences velocity in the opposite direction. The larger the recirculation zone, the more dominant is the increase in speed with a negative vector which triggers a decrease in the pressure coefficient. These conditions can affect the flow efficiency. The excess recirculation zone in the BFS flow shows a lower pressure coefficient; therefore, energy is wasted owing to the formation of the recirculation zone. Meanwhile, in the BFS flow, the slope angle of the pressure coefficient was maintained to minimize the pressure difference between the wall and free-stream. Therefore, the BFS flow with slope angle shows a more efficient flow condition.

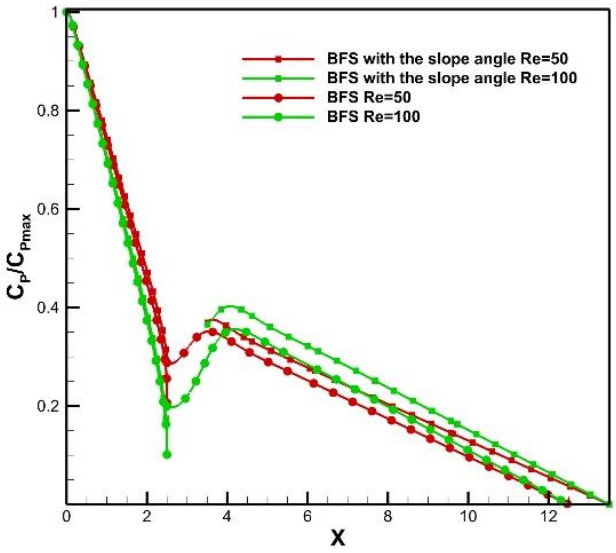

(a) Re=50 and 100

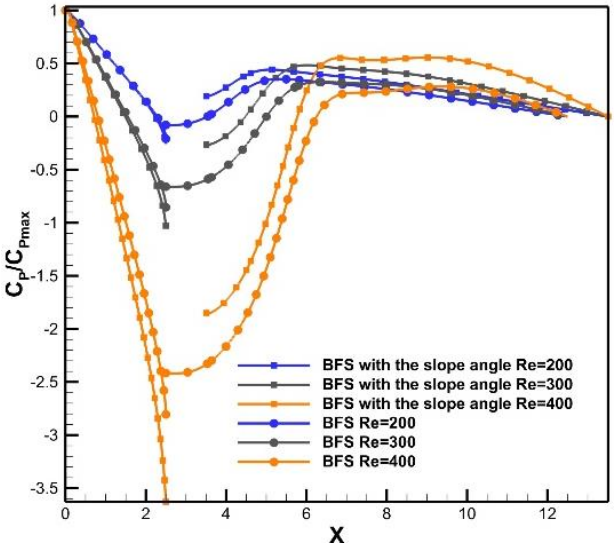

(b) Re=200, 300, and 400

Fig. 9. Graph of C_P normalized by C_{Pmax}.

4 Conclusion

This study investigated the influence of the slope angle of the step on the BFS flow characteristics. The BFS flow was tested using numerical calculations with variations in the Reynolds number, which included Re=50, 100, 200, 300, and 400. The computational results show that the flow separation phenomenon is the main characteristic of the BFS flow. Additionally, this phenomenon provides complex conditions that can affect the flow conditions of the channel. Flow separation triggers a recirculation zone that grows as the Reynolds number increases in a BFS without slope angle. The recirculation zone causes the fluid flow to experience a velocity in the direction oppositeto that of the vector. This condition triggers a pressure difference that is too significant and affects the flow efficiency in the channel. The recirculation zone significantly decreasedunderthe influence of the slope angle of the step. A recirculation zone is formed when Re>100 in the BFS flow with slope angle. In addition tominimizing the increase in the recirculation zone, a BFS with a slope angle can delay the occurrence of flow separation. Based on the friction coefficient, the flow separation point becomes closer to the upstream wall as the Reynolds number increases.

Based on the results of this study, a BFS with an angle of slope can maintain the efficiency of fluid flow through the channel. This condition can be observed in the distribution of the resulting pressure coefficient. Flow separation is critical based on BFS implementation in the industrial world. However, the formed recirculation zone can affect the fluid flow conditions. This indicates that an excessive increase in the recirculation zone can

harm various essential aspects. Therefore, controlling the recirculation zone through the angle of inclination of the steps is very important to maintain fluid flow efficiency, which significantly impacts the industrial world, especially in industries that involve piping, such as oil, gas, and steam power plants.

References

[1] H. A. Mohammed, A. A. Al-aswadi, N. H. Shuaib, and R. Saidur, "Convective heat transfer and fluid flow study over a step using nanofluids: A review," *Renewable and Sustainable Energy Reviews*, vol. 15, no. 6, pp. 2921–2939, 2011, doi: https://doi.org/ 10.1016/j.rser.2011.02.019.

[2] H. U. RuYun, W. Liang, and F. U. Song, "Review of backward-facing step flow and separation reduction," *SCIENTIA SINICA Physica, Mechanica&Astronomica*, vol. 45, no. 12, p.124704, 2015, doi: https://doi.org/ 10.1360/SSPMA2015-00450-176.

[3] P. M. Nadge and R. N. Govardhan, "High Reynolds number flow over a backward-facing step: structure of the mean separation bubble," *Exp Fluids*, vol. 55, no. 1, p. 1657, 2014, doi: 10.1007/s00348-013-1657-5.

[4] Z.-Y. Guo, D.-Y.Li, and X.-G. Liang, "Thermal effect on the recirculation zone in sudden-expansion gas flows," *Int J Heat Mass Transf*, vol. 39, no. 13, pp.2619-2624, 1996, doi: https://doi.org/10.1016/0017-9310(95)00371-1.

[5] K. O'Malley, A. D. Fitt, T. V Jones, J. R. Ockendon, and P. Wilmott, "Models for high-Reynolds-number flow down a step," *J Fluid Mech*, vol. 222, pp. 139–155, 1991, doi: DOI: 10.1017/S0022112091001039.

[6] R. Ruisi, H. Zare-Behtash, K. Kontis, and R. Erfani, "Active flow control over a backward-facing step using plasma actuation," *Acta Astronaut*, vol. 126, pp. 354–363, 2016, doi: https://doi.org/10.1016/ j.actaastro.2016.05.016.

[7] Y. Rouizi, Y. Favennec, J. Ventura, and D. Petit, "Numerical Model Reduction of 2D Steady Incompressible Laminar Flows: Application on the Flow over a Backward-Facing Step," *J. Comput. Phys.*, vol. 228, no. 6, pp. 2239–2255, Apr. 2009, doi: 10.1016/j.jcp.2008.12.001.

[8] E. Erturk, "Numerical solutions of 2-D steady incompressible flow over a backward-facing step, Part I: High Reynolds number solutions," *Comput Fluids*, vol. 37, no. 6, pp. 633–655, 2008, doi: https://doi.org/10.1016 /j.compfluid.2007.09.003.

[9] E. Erturk, T. Corke, and C. Gokcol, "Numerical Solutions of 2-D Steady Incompressible Driven Cavity Flow at High Reynolds Numbers," *Int J Numer Methods Fluids*, vol. 48, pp. 747–774, Jul. 2005, doi: 10.1002/fld.953.

[10] V. Uruba, P. Jonáš, and O. Mazur, "Control of a channel-flow behind a backward-facing step by suction/blowing," *Int J Heat Fluid Flow*, vol. 28, no. 4, pp. 665–672, 2007, doi: https://doi.org/10.1016/j.ijheatfluidflow.2007.04.002.

[11] E. Montazer, H. Yarmand, E. Salami, M. R. Muhamad, S. N. Kazi, and A. Badarudin, "A brief review study of flow phenomena over a backward-facing step and its optimization," *Renewable and Sustainable Energy Reviews*, vol. 82, pp. 994–1005, 2018, doi: https://doi.org/10.1016/j.rser.2017.09.104.

[12] B. Armaly, F. Durst, J. Pereira, and B. Schönung, "Experimental and Theoretical Investigation of Backward-Facing Step Flow," *J Fluid Mech*, vol. 127, pp. 473–496, May 1983, doi: 10.1017/S002211208300283 9.

[13] J. Julian and R. F. Karim, "Flow control on a squareback model," *International Review of Aerospace Engineering*, vol. 10, no. 4, pp. 230–239, 2017.

[14] J. Julian, W. Iskandar, and F. Wahyuni, "Aerodynamics Improvement of NACA 0015 by Using Co-Flow Jet," *International Journal of Marine Engineering Innovation and Research*, vol. 7, pp. 1479–2548, Mar. 2022, doi: 10.12962/j25481479.v7i4.14898.

[15] J. Julian, R. Difitro, and P. Stefan, "The effect of plasma actuator placement on drag coefficient reduction of Ahmed body as an aerodynamic model," *International Journal of Technology*, vol. 7, no. 2, pp. 306–313, 2016.

[16] J. Julian, R. Difitro, and P. Stefan, "The effect of plasma actuator placement on drag coefficient reduction of Ahmed body as an aerodynamic model," *International Journal of Technology*, vol. 7, no. 2, pp. 306–313, 2016.

[17] Harinaldi, Budiarso, and J. Julian, "The effect of plasma actuator on the depreciation of the aerodynamic drag on box model," in *AIP Conference Proceedings*, AIP Publishing LLC, 2016, p. 040004.

[18] J. Julian, W. Iskandar, and F. Wahyuni, "COMPUTATIONAL FLUID DYNAMICS ANALYSIS BASED ON THE FLUID FLOW SEPARATION POINT ON THE UPPER SIDE OF THE NACA 0015 AIRFOIL WITH THE COEFFICIENT OF FRICTION," *Jurnal Media Mesin*, vol. 23, no. 2.

[19] J. Julian, W. Iskandar, and F. Wahyuni, "Effect of Single Slat and Double Slat on Aerodynamic Performance of NACA 4415," 2022.

[20] J. Julian, W. Iskandar, F. Wahyuni, and N. T. Bunga, "Aerodynamic Performance Improvement on NACA 4415 Airfoil by Using Cavity,"*JurnalAsiimetrik: JurnalIlmiahRekayasa Dan Inovasi*, vol. 5, no. 1, Jan. 2023, doi: 10.35814/asiimetrik.v5i1.425 9.

[21] J. Julian, W. Iskandar, F. Wahyuni, and N. T. Bunga, "Characterization of the Co-Flow Jet Effect as One of the Flow Control Devices," *JurnalAsiimetrik: JurnalIlmiahRekayasa&Inovasi*, pp. 185–192, 2022.

[22] F. C. Megawanto, Harinaldi, Budiarso, and J. Julian, "Numerical analysis of plasma actuator for drag reduction and lift enhancement on NACA 4415 airfoil," in *AIP Conference Proceedings*, AIP Publishing LLC, 2018, p. 050001.

[23] J. Julian, W. Iskandar, F. Wahyuni, A. Armansyah, and F. Ferdyanto, "Effect of Single Slat and Double Slat on Aerodynamic Performance of NACA 4415," *International Journal of Marine Engineering Innovation and Research*, vol. 7, no. 2, 2022.

[24] F. C. Megawanto, R. F. Karim, N. T. Bunga, and J. Julian, "Flow separation delay on NACA 4415 airfoil using plasma actuator effect," *International Review of Aerospace Engineering*, vol. 12, no. 4, pp. 180–186, 2019.

[25] F. C. Megawanto, R. F. Karim, N. T. Bunga, and J. Julian, "Flow separation delay on NACA 4415 airfoil using plasma actuator effect," *International Review of Aerospace Engineering*, vol. 12, no. 4, pp. 180–186, 2019.

[26] W. Iskandar, J. Julian, F. Wahyuni, F. Ferdyanto, H. Prabu, and F. Yulia, "Study of Airfoil Characteristics on NACA 4415 with Reynolds Number Variations," *International Review on Modelling and Simulations (IREMOS)*, vol. 15, p. 162, Feb. 2022, doi: 10.15866/iremos.v15i3.21684.

[27] J. Julian, Harinaldi, Budiarso, C.-C. Wang, and M.-J. Chern, "Effect of plasma actuator in boundary layer on flat plate model with turbulent promoter," *ProcInstMechEng G J AerospEng*, vol. 232, no. 16, pp. 3001–3010, 2018.

[28] G. Biswas, M. Breuer, and F. Durst, "Backward-Facing Step Flows for Various Expansion Ratios at Low and Moderate Reynolds Numbers," *J Fluids Eng*, vol. 126, no. 3, pp. 362–374, Jul. 2004, doi: 10.1115/1.1760532.

[29] P. J. Roache, "Perspective: a method for uniform reporting of grid refinement studies," 1994.

[30] F. Danane, A. Boudiaf, O. Mahfoud, S.-E.Ouyahia, N. Labsi, and Y. K. Benkahla, "Effect of backward facing step shape on 3D mixed convection of Bingham fluid," *International*

Journal of Thermal Sciences, vol. 147, p. 106116, 2020, doi: https:// doi.org/10.1016/j.ijthermalsci.2019.106116.